Composite Structures 327 (2024) 117648

Contents lists available at ScienceDirect

Composite Structures

journal homepage: www.elsevier.com/locate/compstruct

Investigating the effect of cure schedules and cure initiators on sustainable composites for large offshore structures

J.R. Pothnis, K. Vélon, G.S. Bhatia, A. Hejjaji, A.J. Comer *

Bernal Institute, School of Engineering, University of Limerick, Limerick, Ireland

ARTICLE INFO

Keywords:
Glass fiber Reinforced Polymer
Thermoplastic infusible resin
Post-Cure
Cure Initiator State
Mechanical behavior
Failure analysis

ABSTRACT

This study evaluates the effect of post-cure schedules and cure initiator form on the mechanical properties of Glass fibre reinforced polymer (GFRP) laminates manufactured using an infusible reactive thermoplastic resin. Tensile, flexural, shear and dynamic mechanical analysis tests were conducted. Fractography was also performed. Specimens fabricated using liquid cure initiator and subjected to an elevated temperature post-cure were the control specimens. Ambient cured specimens decreased by no more than 12% in the case of tensile properties (modulus of 90° specimens) and by $< 14.3\%$ in the case of flexural properties (also modulus in 90° specimens). Furthermore, the difference in mechanical properties of 0° specimens fabricated using a powder cure initiator was observed to be within $\approx 7\%$ of respective properties of control specimens. In the context of fabricating thick laminates for large-size offshore structures, the results suggest that an extended ambient post-cure cycle in conjunction with an initiator in powder form can be employed instead of an elevated temperature post-cure schedule with initiator in liquid form. This is economically beneficial since it eliminates infrastructure required for elevated temperature curing/post-curing. The risk of porosity induced due to liquid-based initiators is also avoided.

1. Introduction

In recent years, countries around the world have focused on reducing greenhouse emissions and have been expanding offshore wind energy farms in an attempt to harvest one of the most important sources of renewable energy [1]. Offshore structures such as wind turbines continue to be scaled-up in size and number as countries move towards becoming carbon–neutral [2,3]. Although wind power generation has increased exponentially, environmental challenges (corrosion, biodeterioration etc.) continue to exist due to the use of conventional materials like steel for the construction of offshore structures [4]. The relatively low fatigue performance of steel, is another important factor driving the search for alternative materials [3]. It has been reported that approximately 30 % of total lifecycle costs are due to operation and maintenance for offshore wind farms [5]. Therefore, the choice of alternative materials can reduce these costs while complying with the structural requirements. The current work is broadly focused on enabling the increased use of polymer composites in offshore floating wind structures and tidal turbine applications. The research also aims to contribute to the development of sustainable composites to promote material recyclability. Towards achieving these objectives, material characterization studies are performed to understand composite behavior under quasi-static and dynamic (fatigue) loading conditions. In this work, material response under quasi-static loading conditions is presented while fatigue characterization studies of the materials is an ongoing activity. Additionally, the study considers the use of industry-relevant fabrication process and cure/post-cure cycles for the realization and processing of test coupons.

Polymer composites on account of their high specific strength, stiffness, fatigue resistance and superior corrosion resistance have been investigated as alternative construction materials for offshore wind energy support structures [6,7]. While composites based on thermosetting resins such as epoxies have been widely employed, their reuse or recyclability is difficult. Therefore, as a further improvement in the choice of materials, composites fabricated using thermoplastic resins are being viewed as potential replacements for thermosets as matrix materials [8–10]. The difficulties associated with the end-of-life management of thermosetting composites can also be overcome by using thermoplastic matrix materials [11,12].

In this context, ARKEMA has introduced Elium® resin, a reactive

* Corresponding author.
E-mail address: Anthony.Comer@ul.ie (A.J. Comer).

https://doi.org/10.1016/j.compstruct.2023.117648
Received 22 June 2023; Received in revised form 6 September 2023; Accepted 21 October 2023
Available online 28 October 2023

methylmethacrylate thermoplastic resin which while possessing the recyclability of traditional melt-processible thermoplastic resins, can be processed at room temperature using established manufacturing methods such as the vacuum assisted liquid resin infusion manufacturing process which is the most practical and widely used option for the realization of large-scale structures [13,14]. This resin has been developed as a viable replacement for composites typically manufactured using epoxy resins with equivalent mechanical properties [13,15]. Furthermore, thermoplastic resins generally possess superior fatigue properties, fracture toughness, and environmental resistance relative to thermosetting resins [16–18]. The weldability of thermoplastics is also a significant advantage [19,20].

A comprehensive review of the mechanical performance of thermoplastic acrylic-based composites has been presented by Obande *et al.* recently [10]. The review indicates that the thermomechanical and mechanical properties exhibited by the composites with Elium resin are competitive with those of epoxy systems. Various studies in literature report on the mechanical performance of composites fabricated using Elium resin such as the impact response of glass/Elium composites by Boumbimba *et al.* and Kinvi-Dossou *et al.* [21,22]. The viscoelastic behavior of glass/Elium and glass/epoxy composites was evaluated by Obande *et al.* [14]. The study showed that the damping characteristics of the Elium-based composites were better than those of epoxy-based composites. In a related study by the same authors, Elium 188 and epoxy resins were determined to have comparable interlaminar shear stress (ILSS) and flexural properties [23].

In another study, the flexural strength of composites fabricated with Elium 150 resin displayed marginally higher flexural strengths than those of composites fabricated with epoxy resin [11]. A comparative study of glass fiber laminates manufactured using Elium 150, epoxy, vinylester, and dicyclopentadiene-based polyester resin revealed that the laminate made using Elium 150 resin had the highest glass transition temperature (T_g) in the dry state of all resins investigated [12]. In the same study, the ILSS value for Elium 150 composites exceeded the ILSS recorded for vinylester and dicyclopentadiene-based polyester matrix composites. Considering that the resin can be processed over a range of temperatures between 20 and 60 °C, the laminate with the thermoplastic matrix was post-cured at ambient temperature (≈ 23 °C). Han *et al.*[24] evaluated the effect of fabrication temperature conditions on the interlaminar shear properties of glass/Elium composites. Laminates were fabricated at room temperature (24 °C), 50 °C and 80 °C. The authors reported improvements greater than 50% in interlaminar shear strength, mode I and mode II fracture toughness due to an increase in fabrication temperature from 24 °C to 80 °C.

By evaluating the quasi-static crush performance of 3D composites, Shah *et al.* [25] concluded that composites with Elium matrix can absorb energy up to 30 % higher as compared to 3-D composites fabricated with an epoxy resin. In a study by Murray *et al.* [26], the flexural behaviour of spar caps made from Elium 188 and epoxy resins were compared. Both resins displayed similar performances in elastic three-point bending tests. A comparative study was performed using a three-point-bend test on tubular carbon fiber composites with Elium and epoxy as matrix materials [27,28]. Both composites exhibited similar load carrying capability but the composite with Elium matrix showed a higher strain-to-failure. The Elium composite structure failed by interlaminar shear and ply-splitting and the composite exhibited ductile failure. The flexural properties of Elium and epoxy composites had very similar flexural moduli, although it was noted that the Elium composite exhibited progressive damage due to the ductile nature of the matrix. The same authors also evaluated the effect of annealing on the flexural performance of Elium composites. While one laminate configuration was annealed at 80 °C for 2 h in a hot press, the other laminate was annealed at room temperature for the same duration. An 11 % and 21 % higher flexural stiffness and flexural strength, respectively, was achieved due to annealing at elevated temperature. The authors attribute the difference to the possibility of reorganizing of microstructure at higher temperature. Further they also discussed the possibility of laminates remaining partially uncured since they were fabricated at room temperature. However, the effect of prolonged annealing at room temperature on the laminate performance was not investigated in the work. A few other studies also report on the comparative behavior of elium-based and epoxy-based composites processed under different cure conditions [9,30]. Raponi *et al.* [29] investigated the effect of varying cure initiator concentration on the polymerization process of the resin employing thermal and rheological analysis methods. In addition, dynamic mechanical analysis (DMA) was performed on the resin samples to determine glass transition temperature. It was reported that a 1.2 % concentration by weight of peroxide resulted in the fastest polymerization time. In addition to thermal stability, the best value of glass transition temperature based on tangent delta peak (123 °C) was also recorded for this initiator concentration. Mechanical properties of the resin samples as a function of cure schedule were however not investigated in the study. It is also evident from literature that the resin system can be recycled and thus facilitate sustainable development of composites. However, previous works from literature indicates the necessity to focus further on process-related research to enhance the adoption-potential of this resin system to fabricate large-scale components in an industrial environment [10].

Elium resin comprises of methylmethacrylate monomer that polymerizes with a peroxide-cure initiator [13]. Aqueous dibenzoyl peroxide liquid cure initiators are widely employed in industry to initiate the cure process for Elium resin, typically processed using the vacuum assisted liquid resin infusion moulding process. However, industry requirements often dictate the need to infuse relatively thick fibre reinforcement preforms (greater than20 mm). In the case of glass fiber preforms, this can be especially challenging due to the exothermic heat build-up during the infusion process and poor heat dissipation considering the low thermal conductivity value of glass fibers (0.8 W/m K). The heat build-up can also trigger the aqueous component of the cure initiator to boil, ultimately leading to porosity in the infused component/laminate. This in turn can result in relatively low laminate mechanical properties. To alleviate this problem initiators in powder form have been introduced. The current study investigates the effect of both aqueous and powder forms of cure initiators on laminate mechanical properties. Additionally, Elium-based composites are often subjected to heated post-cure schedules using a heated tent or by heating the manufacturing building. With increasing component size, heated post-cures are potentially uneconomical. In this regard, we also investigate the mechanical properties resulting from an extended ambient post-cure schedule which is of interest for the manufacture of large structures as elevated cure schedules are difficult and expensive to perform. In the present work, the standard 60 °C post-cure with aqueous form cure initiator is considered as the baseline for comparison. The effect of using different post-cure cycles on the resultant mechanical properties achievable is investigated.

2. Materials and methods

2.1. Materials

Unidirectional (UD) non-crimp glass fabric of areal density 320 gsm (Gerster GmbH and Co. KG, Germany) was the reinforcement used in composite fabrication. The fabric architecture comprised of continuous glass fibres (Hybon^{TM} 2026 1200 tex from Nippon Electric Glass Co., Ltd., Japan) in the warp direction held together by Polyester (PES) fibers in the weft direction. The thermoplastic Elium® 188 XO resin (Arkema, France) with two different types of cure initiators, (a) Perkadox GB-50X (powder) and b) BP-40-SAQ (liquid) was used as the matrix material. Elium is a Methyl Methacrylate (MMA)-based resin and polymerizes with the aid of a cure initiator to form polymethylmethacrylate. Benzoyl peroxide (BPO) is a radical cure initiator used to induce polymerisation and it can either be in powder or water-based forms. In this study, both forms of BPO cure initiator were employed. The mix ratio of the resin

and the cure initiators was 100:3 by weight for both forms of the cure initiator. A key consideration for the choice of this matrix system was its processability at ambient temperature enabling the fabrication of large-sized structures. Furthermore, the use of this matrix system potentially allows recycling of composites thus contributing to the development of sustainable composites.

2.2. Composite fabrication and specimen preparation

Two UD laminates comprising of 10 layers each ($[0]_{5s}$) were manufactured using a vacuum assisted liquid resin infusion moulding process. While one laminate was fabricated using powder cure initiator, the other was fabricated using a liquid cure initiator. Fig. 1 presents the arrangement employed for fabricating the laminates. Once the infusion process was completed, the composite laminates were cured for 24 h at ambient temperature. Subsequently, the laminates were removed from the infusion set-up and specimens for the different tests were carefully extracted from the laminates using a water-cooled diamond coated rotating disc-cutter. Specimen dimensions were obtained from the corresponding test standards [30–32].

The extracted specimens were then segregated into four different batches with each batch having a unique combination of post-cure schedule and powder/liquid cure-initiator used during laminate fabrication. A minimum of three replicas were tested from each specimen type in directions along (0°) and across (90°) the fiber axis. Based on the post-cure cycles, the specimens were categorized into four types: (a) High temperature post-cure - powder initiator (HTP), (b) High temperature post-cure - liquid initiator (HTL), (c) Ambient temperature post-cure - powder initiator (ATP) and (d) Ambient temperature post-cure - liquid initiator (ATL). While the HTP and HTL specimens were subjected to a post-cure at 60 °C for 2 h, the ATP and ATL specimens were subjected to an ambient post-cure (approximately 20 °C) for a minimum period of 11 weeks. The duration of ambient post-cure cycle was chosen such that it was of a sufficiently long duration as compared to that of elevated temperature post-cure cycle and also based on typical turnover times available between component manufacturing and installation in industrial applications. Fiber volume fraction of the composites was evaluated as per ASTM standard D3171-15 [33] and was found to be ≈ 52 % for the laminates fabricated. In this study, the HTL specimens were the control samples.

2.3. Mechanical testing

2.3.1. Tensile testing

Tensile properties of specimens were evaluated for the various specimen types both along (0°) and across (90°) the fiber direction as per ISO 527–5 (2009) standard [30]. The specimens were strain gauged along the longitudinal and transverse directions relative to the applied load and the measurements were recorded using a data acquisition DAQ system (Model 8000, Vishay Micro Measurements). The tests were performed on a Zwich/Roell RK hydraulic testing machine with a 100kN load cell under displacement-controlled conditions of 1 mm/min. Fig. 2 (a) shows a typical specimen subjected to tensile testing.

2.3.2. Three-point bending testing

Three-point bending tests were performed on specimens in accordance with ISO 14125 (1998) standard [31]. The flexural tests were performed on a Tinius Olsen universal testing machine (UTM) fitted with a 10kN load cell. Both 0° and 90° specimens were tested for each type of laminate. Fig. 2(b) shows a typical specimen subjected to flexural loading. The nominal dimensions of the specimens were 100 mm × 15 mm × 2.5 mm (length × width × thickness). A span to thickness ratio of 20 was used for the tests. A crosshead speed of 1 mm/min was maintained during the tests. While the loading roller was 10 mm in diameter, the support rollers were 4 mm in diameter.

2.3.3. Short beam shear tests

ISO 14,130 (1997) [32] was the reference standard used to conduct

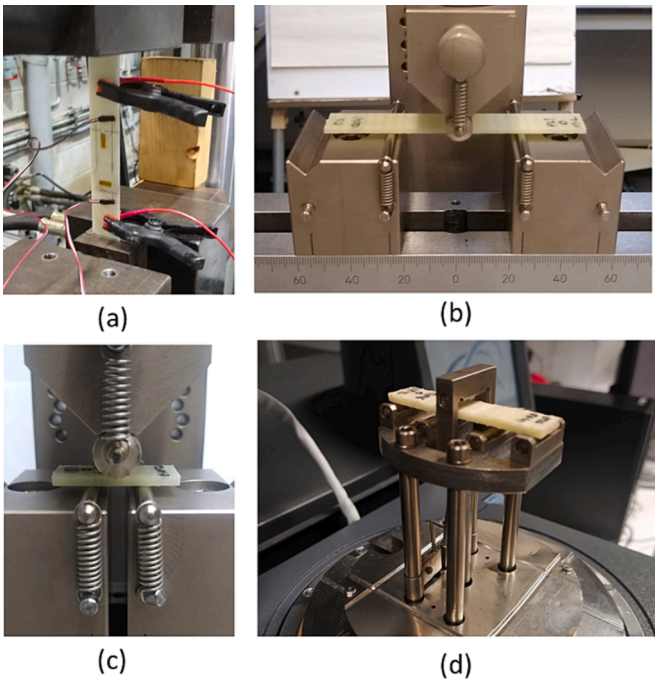

Fig. 2. Experimental set-up employed for various tests (a) tension test, (b) three-point bending test, (c) short beam shear test, (d) three-point bending test fixture for DMA testing.

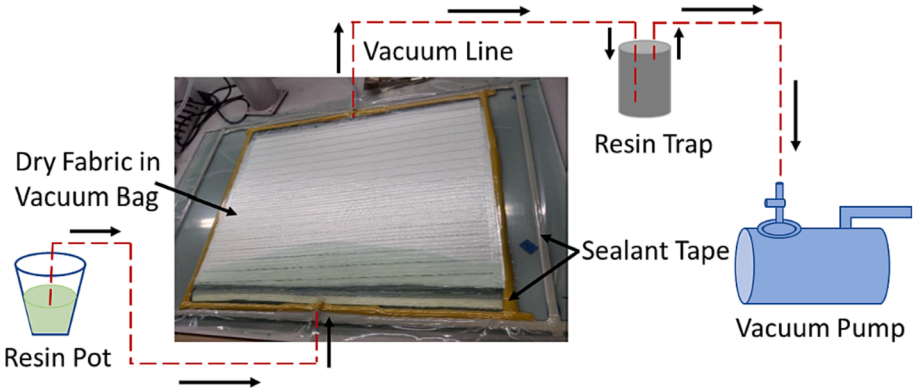

Fig. 1. Vacuum assisted liquid resin infusion setup for laminate fabrication.

short beam shear (SBS) tests to determine the interlaminar shear strength (ILSS) of the composites fabricated. The set-up employed for flexural testing was also used to conduct the SBS tests. Again, three replicas of specimens were tested from each specimen type. However, in these tests, only specimens with fibers aligned along the span direction were tested. Fig. 2(c) shows a typical specimen subjected to SBS testing. The loading and support rollers were the same that were used during flexural tests. The nominal specimen dimensions were 30 mm × 15 mm × 2.5 mm (length × width × thickness) and a span to thickness ratio of 5 was used for the experiments. A test speed of 1 mm/min was employed for the tests.

2.3.4. Dynamic mechanical analysis

In addition to the tensile, flexural and shear properties, specimens were also evaluated using dynamic mechanical analysis (DMA). Considering the varied post-cure cycles and cure initiators used during composite fabrication, storage modulus (E'), loss modulus (E'') and glass transition (T_g) of specimens drawn from the different types was determined over a range of temperatures up to 150 °C. The viscoelastic behavior of the composites were determined using a three-point bending test configuration (Model Q800, TA Instruments). The nominal specimen dimensions were 60 mm × 12 mm × 2.5 mm (length × width × thickness) and three specimens of each type were tested. A heating rate of 3 °C/ min was used and the tests were performed at a frequency of 1 Hz. Fig. 2(d) shows a specimen mounted in the DMA test fixture prior to testing.

2.3.5. Fractography of tested samples

Fracture surfaces of select specimens tested under tensile, flexural and shear loading conditions were studied using a Hitachi SU-70 high-resolution scanning electron microscope (SEM). Prior to SEM analysis, the specimen surfaces to be examined were sputter coated with gold for 90 s using an Emitech K550 sputter coater. In the case of specimens examined on the through-thickness side (flexure and interlaminar shear specimens), the specimens were mounted in a two-part epoxy system (Epoxicure resin-hardener) with a conductive filler added to it. The mounted specimen surfaces were ground and polished prior to SEM analysis.

3. Results and discussion

The mechanical properties of UD glass fiber/Elium 188XO laminates manufactured using two different cure initiators and subjected to two different post-cure processes were evaluated. Table 1 presents a summary of the different tests conducted including the fiber orientation of the specimens as part of this study. Specimens fabricated with liquid cure initiator and subjected to a heated post-cure cycle (60 °C for two hours) were the control samples in the present study.

Table 1
Details of cure initiators, post-cure cycles and specimens tested. First row in the table refers to control samples.

Cure initiator	Post-cure cycle	Specimen reference	Test specimens with fiber orientation relative to load applied	
			0°	90°
Liquid	Heated (60 °C) for 2 h	HTL	Tensile, Flexure, SBS, DMA	Tensile, Flexure
Liquid	Ambient temperature (≈ 20 °C) for a minimum of 11 weeks	ATL	Tensile, Flexure, SBS, DMA	Tensile, Flexure
Powder	Heated (60 °C) for 2 h	HTP	Tensile, Flexure, SBS, DMA	Tensile, Flexure
Powder	Ambient temperature (≈ 20 °C) for a minimum of 11 weeks	ATP	Tensile, Flexure, SBS, DMA	Tensile, Flexure

3.1. Tensile properties

Fig. 3 presents stress–strain plots obtained for the specimens tested. While the plots in Fig. 3(a) were obtained from specimens with 0° fiber orientation, Fig. 3(b) presents plots from representative specimens with 90° fiber orientation with respect to the loading direction. Referring to Fig. 3(a), the strength and failure strain values of specimens fabricated with liquid initiator was observed to be marginally higher (<5 %) as compared to those fabricated with powder initiator. The tensile modulus of the laminates was measured to be in the range of ≈37-39 GPa for the 0° specimens tested. The failure strain values ranged from 2.25 % to 2.75 % for the 0° specimens. Considering that the loading direction is fiber-dominant, the strength values for the different specimen types varied within 7 % of their respective values with respect to that of the control samples. Additionally, the effect of post-cure temperature on the measured tensile strength was minimal. Further, no clear influence of initiator type on the measured tensile properties could be observed with the stress–strain curves being nearly the same. The longitudinal tensile strength and moduli across the four specimen types are comparable to those reported in the literature [23].

Table 2 summarizes the tensile strength and stiffness values obtained for the specimens tested. In addition to the tensile strength and stiffness, the poissons ratio of the laminates was determined from the strain gauge data and determined to be in range of 0.29–0.32 for the 0° specimens and 0.09–0.11 for the 90° specimens, respectively. In the case of 90° specimens, the modulus values of HTP specimens were ≈ 6 % lower with respect to that of the control samples. However, the difference was lower in case of ATP specimens (<3%). Considering ATL specimens, the tensile modulus was significantly lower (<12%) than the control. The ATP and ATL specimens exhibited greater strains to failure (≈ 25% higher failure strains as compared to those of HTP and HTL specimens). The observed values are possibly due to the ambient cure profile. Although the respective tensile modulus was lower than that of the control, the HTP and ATP 90° specimens exhibited over 24 % higher tensile strength as compared to HTL specimens. Considering the matrix-dominant failure seen in case of the 90° specimens, the effect of post-cure cycles is seen to influence the mechanical strength and strain values obtained. Therefore, the fracture surfaces of select specimens was further examined using SEM for a better understanding of the properties obtained and the results are discussed in Section 3.5. The tensile properties measured indicate that use of ambient post-cure conditions during fabrication can enable achievement of properties comparable to those of the control samples.

3.2. Flexural properties

Representative stress–strain plots obtained from the specimens tested under three-point flexural loading is presented in Fig. 4(a) and 4 (b) for the 0° and 90° specimens (fiber orientation with respect to span), respectively. Considering the various specimen types, the difference in nominal flexural strength was within ≈ 3%. The maximum flexural strength in the 0° orientation was observed in the case of HTL specimens. As compared to ATL specimens, the scatter in strength values was higher for the specimens subjected to elevated post-cure. The flexural modulus of 0° HTL specimens were found to be approximately 14–19 % lower as compared to that of ATP and ATL 0° specimens. However, the flexural modulus of HTP specimens was marginally lower than the control values. Considering the different types of 0° specimens, the nominal modulus values ranged from 21 GPa to 26 GPa in the present work. The ATL 0° specimens displayed the maximum flexural stiffness. This is again attributed to post cure schedules employed, likely leading to a difference in the fiber–matrix interfacial interactions. Table 3 summarizes the flexural test results in the present study. Overall, for 0° specimens, the failure strain values ranged from 3.9 % to 4.3 % across specimen types. The observations are also attributed to a difference in

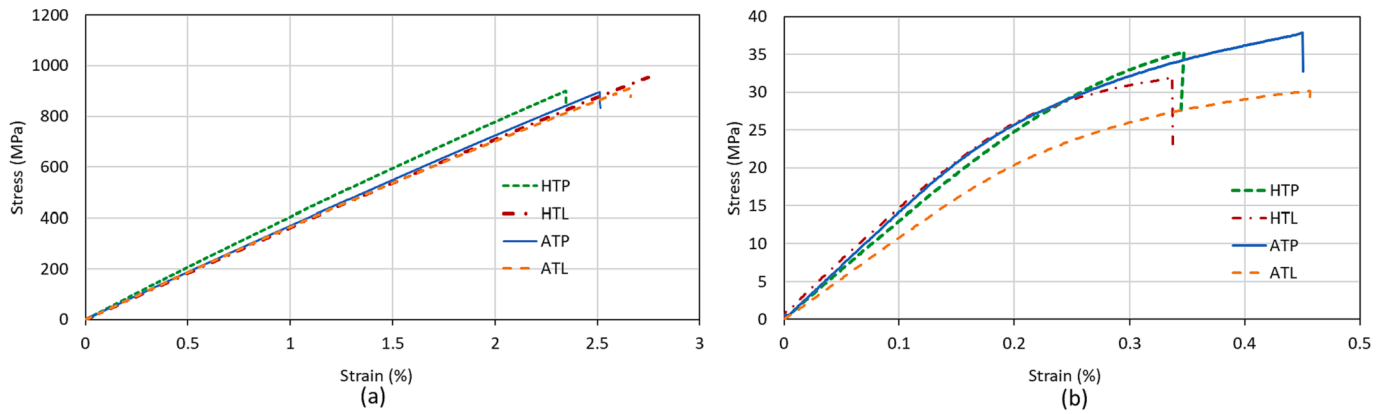

Fig. 3. Typical stress–strain plots obtained from tensile tests (a) fibers oriented along loading direction (0°), (b) fibers oriented transverse to loading direction (90°). Note: HT and AT in figure refer to Post Cure at High Temperature and at Ambient Temperature, respectively. The suffixes P and L refer to Powder and Liquid cure initiators, respectively.

Table 2
Tensile test results. First row in the table refers to control samples.

Specimen reference	Tensile strength (MPa)		Tensile modulus (GPa) and Poisson's ratio (ν_{12})		Difference in average value with respect to control (%)			
	0°	90°	0°	90°	Strength		Modulus	
					0°	90°	0°	90°
HTL	965 ± 20	28.9 ± 2.9	38.3 ± 1.5 0.29 ± 0.02	10.1 ± 1.7 0.09 ± 0.01	—	—	—	—
ATL	921 ± 22	28.3 ± 1.8	36.9 ± 0.8 0.30 ± 0.01	8.9 ± 0.3 0.09 ± 0.00	−4.5	−2.0	−3.6	−11.9
HTP	910 ± 27	37.3 ± 1.9	39.1 ± 1.3 0.29 ± 0.03	9.5 ± 2.3 0.11 ± 0.01	−5.6	+29.1	+2.0	−5.9
ATP	900 ± 08	35.9 ± 2.2	38.5 ± 1.4 0.32 ± 0.01	9.8 ± 0.4 0.11 ± 0.00	−6.7	+24.2	+0.5	−2.9

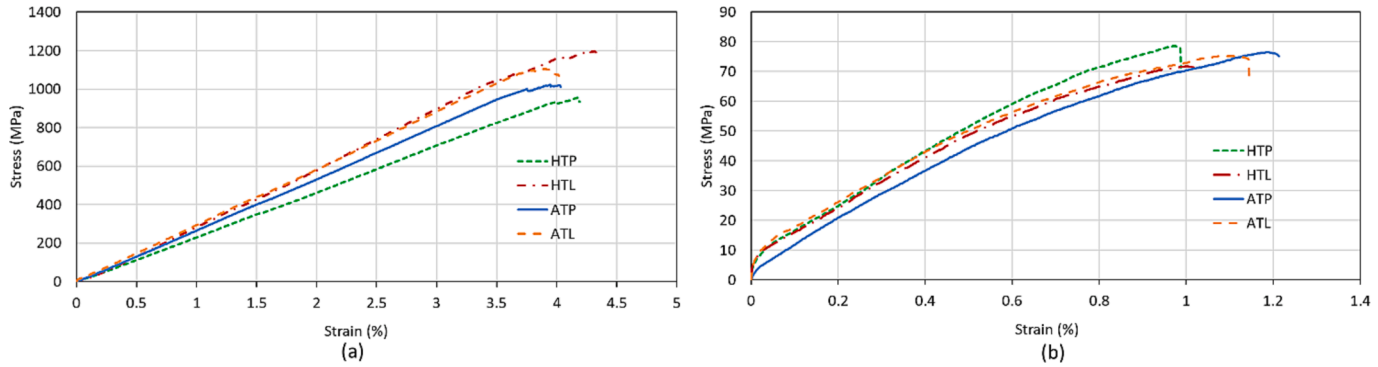

Fig. 4. Typical stress–strain plots obtained during flexural testing (a) fibers oriented along the span, (b) fibers oriented transverse to span. Note: HT and AT in figure refer to Post Cure at High Temperature and at Ambient Temperature, respectively. The suffixes P and L refer to Powder and Liquid cure initiators, respectively.

fiber–matrix interfacial interaction in case of the different specimen types. Similar to tensile test results, a noticeable difference was observed in flexural strain to failure between HTL and ATL 90° specimens with the latter exhibiting higher failure strains. For the 0° specimens, the strength values of HTL specimens (control) were slightly higher as compared to those of all other specimen types. In the case of 90° specimens, a significant difference in strength values between HTL and HTP specimens was recorded. The nominal flexural strength of HTP 90° specimens was approximately 28 % higher as compared to that of the control samples. Similarly, the flexural strength values of both ATL and ATP 90° specimens were also higher (greater than6%) as compared to the flexural strength of the control samples. Considering modulus values, while ATL and the control specimens exhibited similar values, the values of ATP 90° specimens were significantly lower (<14%) as compared to that of the control. Based on the results, the HTP and ATP specimens are likely to have experienced a slightly weaker fiber–matrix-interfacial interaction leading to lower levels of flexural strength and stiffness. For further assessment of the observed properties, select test specimens were studied using SEM. Overall, the flexural strength values in this study exceeded those reported in literature previously [23].

3.3. *Interlaminar shear properties*

The short beam shear test relies on the generation of interlaminar shear indirectly through bending and allows the determination of the apparent interlaminar shear strength [34]. The peak load value obtained

Table 3
Flexure test results. First row in the table refers to control samples.

Specimen reference	Flexural strength (MPa)		Flexural modulus (GPa)		Difference in average value with respect to control (in %)			
	0°	90°	0°	90°	Strength		Modulus	
					0°	90°	0°	90°
HTL	1134 ± 62	65 ± 6.6	21.7 ± 0.5	9.8 ± 0.7	—	—	—	—
ATL	1072 ± 32	70 ± 5.1	25.9 ± 1.6	9.8 ± 0.6	−5.4	+7.6	+19.3	0
HTP	1053 ± 97	83 ± 4.9	21.0 ± 1.6	10.1 ± 0.6	−7.1	+27.7	−3.2	+2.0
ATP	1094 ± 73	69 ± 7.3	24.7 ± 1.9	8.4 ± 0.2	−3.5	+6.1	+13.8	−14.3

from load-displacement curves was considered for the determination of interlaminar shear strength. These values for the different specimen types were in the range of 2400 N to 2600 N. The ATL specimens registered lower peak load compared to both HTL and HTP specimens (≈ 5.5–7 % lower). The reported average values are presented in Table 4. Subsequently, the ILSS values were determined and the ILSS values of the four specimen types were in the range of 49 – 52 MPa. The tested specimens were observed using SEM. In addition to fiber breakage beneath the loading pin, micro cracks were also observed in the specimens. The observation of shear bands in the specimens during testing indicated that specimen failure occurred primarily on account of interlaminar shear stresses (see Fig. 10). Further details on the specimen failure are discussed in Section 3.5.

3.4. Dynamic mechanical analysis

The results from DMA testing for a typical specimen is presented in Fig. 5. The variation of storage modulus (E'), loss modulus (E'') and tan delta values with increasing temperature was determined to estimate the glass transition temperature (T_g) of the matrix system. Considering that the matrix system is investigated for its utility in structural applications, a conservative estimate of T_g values is considered. Therefore, the T_g value obtained from the plot showing E' as a function of temperature is used. The value is determined as the intercept of two lines; the line tangential to the plateau region of the storage modulus and the second line is tangential to the line indicating a sudden drop of storage modulus in the transition region. The T_g values from the loss modulus and tan delta curves correspond to their respective peak values in their respective plots. A summary of T_g values obtained in the case of the different specimens tested is presented in Table 5. From the E' curves, the T_g values were observed to be in the range of 76 °C to 82 °C with the highest average value recorded for the ATL specimens. An ambient temperature post-cure is seen to produce a slightly higher E' value as compared to the elevated temperature post-cure in the case of liquid cure initiator. This is possibly due to small differences in the overall cure state of the specimens processed under different post-cure conditions. Similarly, a small difference in T_g for specimens was observed in the case of HTP and ATP specimens. However, the overall observation as seen from Table 5 was that the difference was not significant.

Table 4
Interlaminar shear test results. First row in the table refers to control samples.

Specimen reference	Interlaminar shear stress (ILSS) (MPa)	Difference in average ILSS value with respect to control (%)
	0°	
HTL	52.2 ± 1.1	—
ATL	48.5 ± 1.5	−7.1
HTP	49.7 ± 2.5	−4.7
ATP	51.2 ± 2.2	−1.9

3.5. Fractography of specimens characterized using different loading conditions

Based on the outcome of tensile, flexural and shear tests performed, it was observed that the choice of cure initiator (powder/liquid) had a minimal negative effect on the properties measured apart from the reduction in flexural modulus in ATP 90° specimens as compared to that of the control. Further, the mechanical properties based on the use of ambient or elevated post cure cycles were also comparable apart from the drop in flexural modules of ATP 90° specimens (-14.3%) and tensile modulus of ATL 90° specimens (-12%) as compared to that of the control. To gain further insight and add to the observations made using macroscopic testing, fractography was performed on select test specimens. Specimens manufactured using liquid initiator were chosen for the SEM study as the main focus was on the effect of post cure temperature (ambient/elevated) on the failure mechanisms. Specimens from tensile, flexure and short beam shear tests were examined. Further, based on the strength values across the tests for specimens fabricated with powder and liquid cure initiators and also on the use of ambient or elevated post-cure cycle employed, HTL and ATL specimens were chosen for examination using SEM.

Fig. 6 (a) and 6 (b) present typical tensile tested failed specimens and drawn from 0° and 90° fiber orientations, respectively. Inspection of the 0° specimens revealed extensive separation of fibers along the longitudinal direction and fiber breakage. In the case of 90° specimens, failure was localized leading to specimen fracture within the gauge area. In both specimens, delamination damage was also observed. Fig. 7(a) and 7 (b) presents the fracture surfaces observed in 0° specimens drawn from HTL and ATL specimens, respectively. Specimen fracture surfaces were observed as per the schematic included in Fig. 7(s1) and 7(s2). Extensive plastic deformation of the thermoplastic matrix was seen in HTL specimens (refer Fig. 7(a2)) and slightly lesser in case of ATL specimens (refer Fig. 7(b2) [24]. The presence of river patterns on fracture surface could be noticed (refer Fig. 7(a1)) similar to that observed in a study reported earlier [8]. This is also evident from the strains to failure as seen in Fig. 3 (a) (≈6 % higher strains seen in HTL specimens as compared to ATL specimens). The HTL specimen exhibited the highest strain to failure. Matrix adhesion to fibers was seen in both cases. However, the ATL specimen showed cleaner fiber surfaces perhaps suggesting slightly weaker fiber–matrix bonding. Thus possibly, the ATL and ATP specimens registered lower failure strains (≈4.5 % and ≈9 % lower, respectively) as compared to HTL 0° specimen. The HTP specimen although exhibited higher stiffness values, the strain to failure was the least. This points to a strong fiber–matrix bonding but the presence of defects locally is likely to have caused specimen failure at a lower strain level. Separation at fiber–matrix interface was evident in both the cases. It has been reported that failure in UD glass fiber composites can occur due to adhesive failure between the matrix and the fibers. Therefore, it is

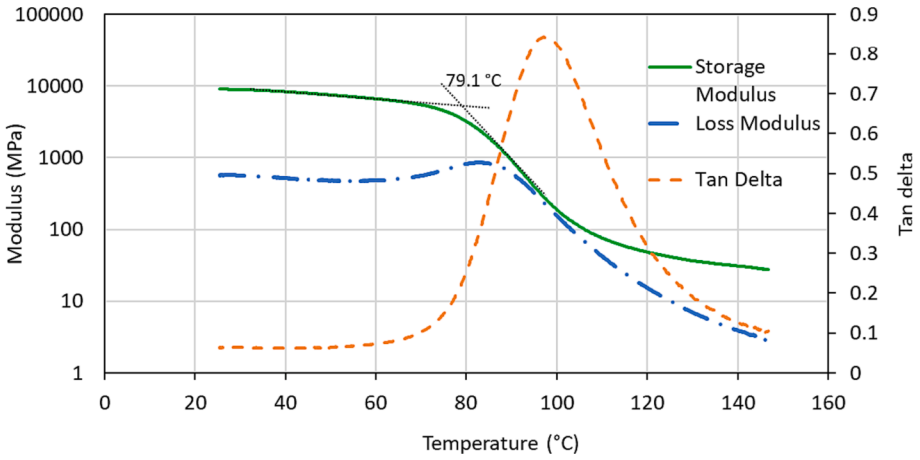

Fig. 5. DMA test results obtained for a HTP specimen subjected to a temperature ramp and using three-point bending fixture in DMA.

Table 5
Dynamic mechanical analysis test results. First row in the table refers to control samples and T_g value from E' curve considered for comparison.

Specimen reference	Glass transition temperature (T_g) (°C)			Difference in average T_g value with respect to control (%)
	E' curve	E'' curve	Tan delta curve	
HTL	80.6 ± 1.1	84.1 ± 1.1	100.4 ± 0.3	—
ATL	81.2 ± 2.0	81.5 ± 1.3	101.0 ± 2.1	+0.2
HTP	79.4 ± 1.0	82.9 ± 0.1	97.6 ± 0.3	−1.4
ATP	76.2 ± 1.1	78.1 ± 0.5	96.7 ± 0.7	−5.4

important to have a strong interface. In the present case, the adherence of matrix material on the fibers after failure indicates a strong bond between the composite constituents. Fig. 7(c) and 7 (d) correspond to the 90° specimen surfaces from HTL and ATL specimens, respectively. The lumpy and jagged matrix surfaces is attributed to Mode I failure of the tensile specimens and is indicative of cohesive failure of the matrix. The fracture surfaces were uneven and rough (refer Fig. 7 (c2) and 7 (d2)). Even in this case, the fiber surfaces of the ATL specimen were found to be smoother with lesser matrix adhesion. Evidence of matrix plastic deformation and fiber separation at the interface was also seen.

Fig. 8 (a) and 8 (b) show typical 0° and 90° failed flexural specimens, respectively. Both, compression side and tension side of typical 0° flexural specimens is presented in Fig. 8 (a). Similarly, typical 90° specimens are presented in Fig. 8 (b). In the case of 0° specimens, the specimens revealed damage beneath the loading pin on the compression side of the specimens. Delamination damage and fiber breakage was also observed on the tension side of the specimens as seen in Fig. 8 (a). However, the extent of visible damage was less obvious in the case of 90° specimens

Fig. 6. Typical tensile test specimens after testing (a) fibers in specimens oriented along loading direction (0° specimens), (b) fibers oriented transverse to loading direction (90° specimens) with locations of final failure indicated.

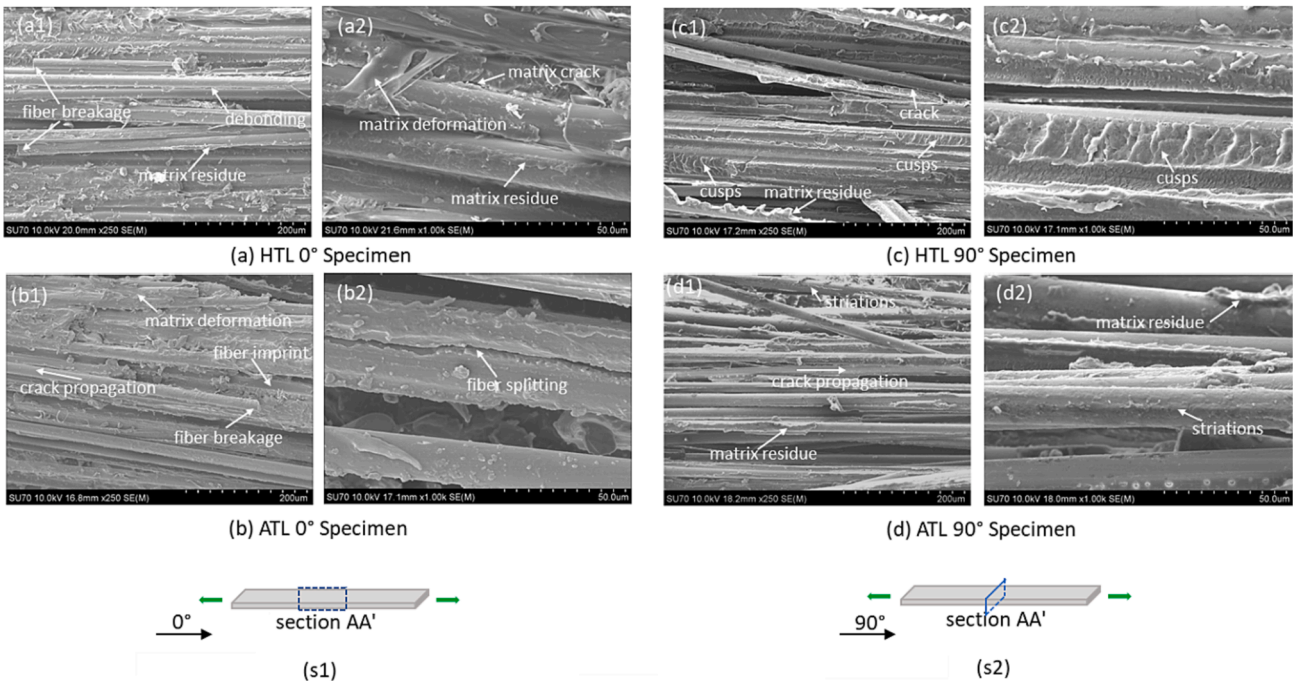

Fig. 7. SEM images corresponding to fracture surfaces of tensile specimens fabricated with liquid initiator (a) HTL 0° specimen, (b) ATL 0° specimen, (c) HTL 90° specimen, (d) ATL 90° specimen. (s) schematics showing section planes for viewing in SEM (s1) in 0° specimens, (s2) in 90° specimens with respective fiber orientation.

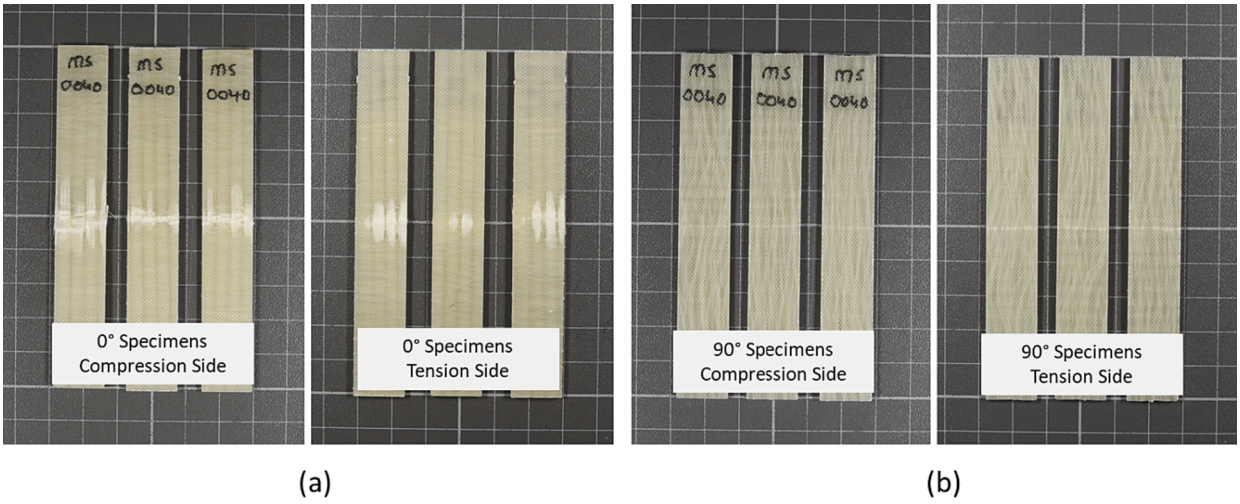

Fig. 8. Typical flexural test specimens after testing (a) fibers in specimens oriented along the span (0° specimens) (b) fibers oriented transverse to span (90° specimens).

(Fig. 8 (b)). Fig. 9 (a) and 9 (b) show details of failed HTL and ATL specimens, respectively as viewed in the thickness direction. Fig. 9 (s1) and 9 (s2) indicate the regions of the specimens examined using SEM. Fiber breakage, delamination and crack initiation points can be observed. The fracture features were similar in both the specimens. The specimens were observed to be damaged approximately to a depth of 4 reinforcement layers on the compression side and to an approximate depth of 3 reinforcement layers on the tension side. Damage was especially pronounced in the region beneath the loading pin. Fiber buckling / kinking was clearly evident as seen in Fig. 9 (a1) and 9(b1). Fig. 9 (c) and 9 (d) provide details of the fracture surfaces of 90° specimens. The images in case of HTL 90° specimen correspond to the region closer to the tension side of the specimens. Similarly, Fig. 9 (d) focuses on a ATL 90° specimen with Fig. 9 (d1) and 9(d2) showing regions closer to the specimen surface and on the compressive side of the flexural loading. Matrix cracking, separation of fibers and fiber breakage was observed. Matrix adhering to the fibers was more obvious in case of the HTL specimen compared to ATL specimen as evidenced in Fig. 9 (c2) and 9 (d2).

The HTL and ATL specimens tested under shear loading were also observed under the SEM in the specimen thickness direction. Fig. 10 presents all the four types of short beam shear specimens tested. The formation of shear bands offset from the loading pin location were commonly seen in the tested specimens suggesting that specimen failure was primarily due to interlaminar shear stress. The specimen cross-sections were further examined using SEM to understand the failure mechanisms. The reinforcement layer numbers are approximately identified (see Fig. 11 (a1), 11 (a2) and 11 (b1)) to gauge the extent of

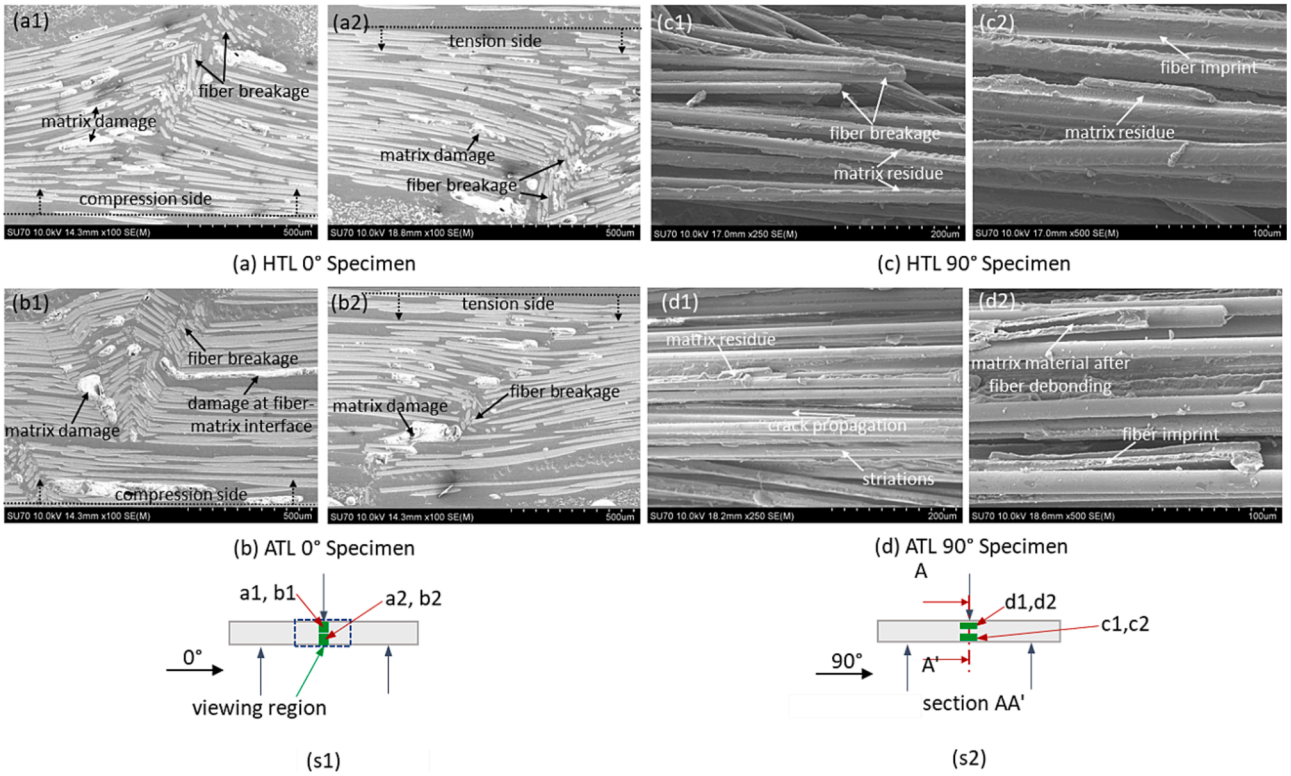

Fig. 9. SEM images from failed flexural specimens fabricated with liquid initiator (a) HTL 0° specimen, (b) ATL 0° specimen, (c) HTL 90° specimen with (c1), (c2) showing regions closer to the specimen surface and on the tensile side of flexural loading, (d) ATL 90° specimen with (d1), (d2) showing regions closer to the specimen surface and on the compressive side of flexural loading, (s) schematics showing section planes for viewing in SEM (s1) in 0° specimens, (s2) in 90° specimens with respective fiber orientation. The approximate specimen locations of images (a1), (b1) and (a2), (b2) are indicated in (s1) and for images (c1), (c2) and (d1), (d2) in (s2).

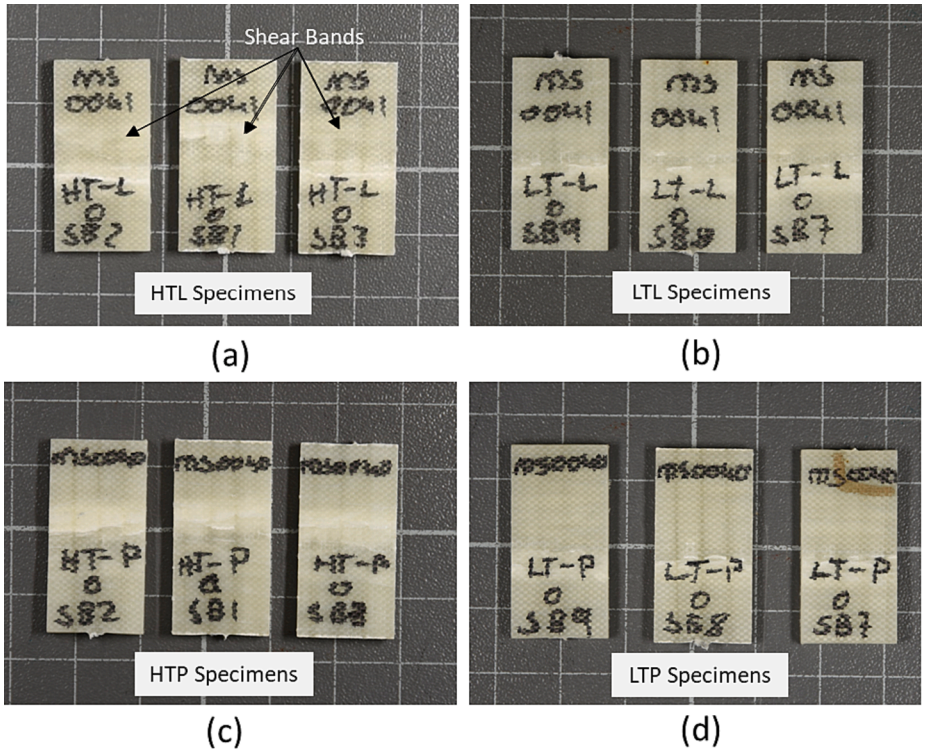

Fig. 10. Typical short beam shear test specimens after testing.

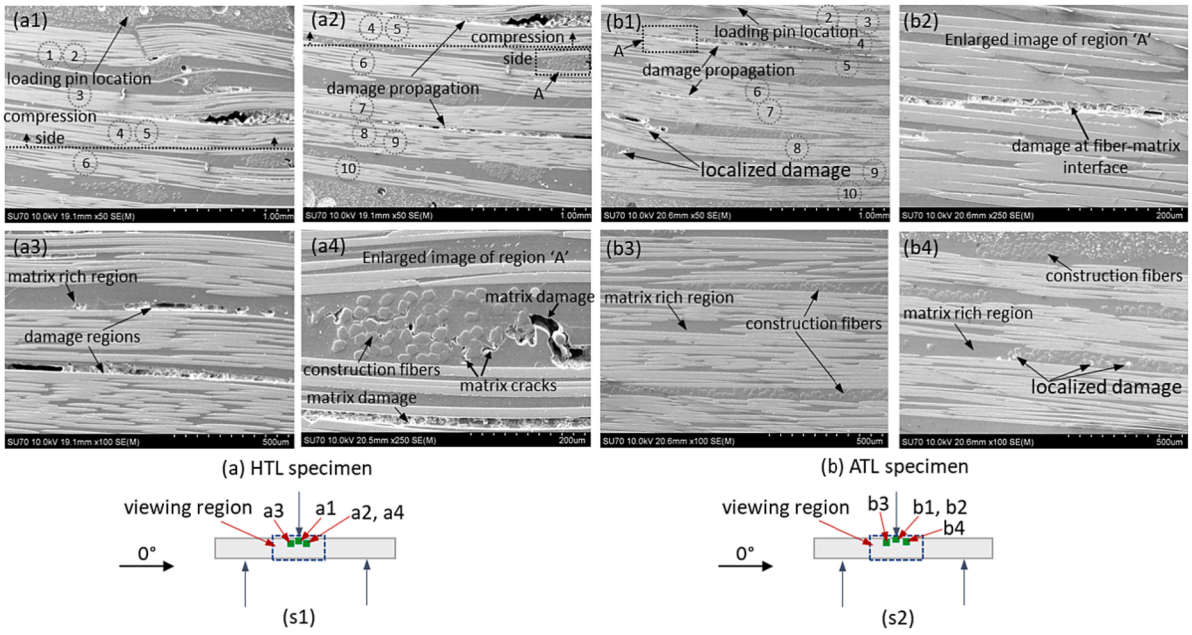

Fig. 11. SEM images from failed ILS specimens fabricated with liquid initiator (a) HTL 0° specimen with (a3) and (a4) showing regions left side and right side of loading pin, respectively, (b) ATL 0° specimen with (b3) and (b4) showing regions left side and right side of loading pin, respectively, (s1) and (s2) schematics showing viewing regions in SEM with specimen fiber orientation in HTL and ATL specimens, respectively. The approximate specimen locations of images (a1) to (a4) and (b1) to (b4) are indicated in (s1) and (s2), respectively.

damage in the specimens. The loading pin location is indicated in the images and damage in specimens was also observed to occur beneath the loading pin. Damage was seen to occur more extensively in the case of the HTL specimen as seen in Fig. 11 (a1) to (a4) within the layers and also in the inter-ply resin rich regions. A schematic showing the regions of interest in the specimen for SEM is included as Fig. 11 (s1) and 11(s2). Fig. 11 (a1) to (a4) and 11 (b1) to (b4) present the SEM images from failed ILS HTL and ATL 0° specimens as shown. The schematics showing viewing regions in SEM with specimen fiber orientation in HTL and ATL specimens, respectively are given in Fig. 11(s1) and 11(s2). Evidence of broken fibers, matrix cracks in interlaminar region at several locations was observed in the HTL specimen. Cracks were seen to propagate through the construction fibers. Localized damage was also observed in regions on either side and away from the loading pin location in the case of HTL specimen. The extent of damage was lower in the case of ATL specimen with damage restricted to the region below the loading pin across the thickness as seen in Fig. 11 (b1) and 11 (b2). Regions away from the loading pin on either side were less prone to damage as compared to the HTL specimen (refer Fig. 11 (b3) and 11 (b4)). In the absence of voids, the ILSS value is dependent on the interfacial bond strength between the fibers and matrix. A stronger bond would improve the load transfer between the composite constituents and enhance the shear strength [35,36]. In the present study, the range of ILSS values reported indicate that the influence of post-cure cycle on void formation and interfacial strength was minimal. Assessing the fracture features of the specimens drawn from across the different loading conditions indicates that the failure in HTL and ATL specimens are similar and failure was observed in the interlaminar regions.

4. Conclusions

The effect of using two different post-cure cycles on glass fiber/Elium composites fabricated with either powder or liquid cure initiators was investigated in the current work. The objective was to study the viability of using an extended ambient temperature post-cure cycle in conjunction with a powder initiator for the manufacture of large-sized marine composite structures using a thermoplastic matrix and glass fibre reinforcement. The following conclusions were drawn based on the results obtained:

1. Based on the E' curve, the T_g values were determined to be in the range of 76 °C to 82 °C for the different cases considered. Therefore, the effect of cure initiator type and post-cure cycle on the observed glass transition temperature (T_g) values was observed to be minimal for the laminates and conditions considered in this study.
2. The tensile, flexural and interlaminar shear properties of the specimens evaluated suggest that the mechanical performance of composites cured under an extended ambient temperature is comparable and competitive with respect to the baseline specimens cured at an elevated temperature (60 °C for two hours). However, a reduction of up to 12% (ATL 90° tensile modulus) and 14% (ATP 90° flexural modulus) as compared to that of the control was apparent and this requires important consideration during the design process. This has important implications for the economic manufacture of large composite structures.
3. Marginal difference (apart from ATP 90° flexural modulus at −14% relative to control) was observed in mechanical properties based on the form of the cure initiator. Powder initiator samples dropped off by no more than 7% in the case of tensile properties and no more than 14.3% in the case of flexural properties (90° modulus) suggesting that the powder form cure initiator is a promising alternative to water-based initiator which can be problematic in terms of creating porosity when used in conjunction with thick glass fibre preforms.
4. Fractography of specimens generally indicates strong fiber–matrix adhesion in the composites. Further, cohesive failure was predominantly observed following extensive plastic deformation of the thermoplastic matrix.

Overall, powder-based initiators in conjunction with an extended cure cycle at ambient temperature could allow reactive thermoplastics to be extensively employed for the economic manufacture of thick glass-based laminates in large offshore structures. Further, the cost-savings and reduced infrastructure requirements associated with ambient cure

schedules makes the reactive thermoplastic matrix system attractive for industrial applications.

CRediT authorship contribution statement

J.R. Pothnis: Investigation, Data curation, Validation, Writing – original draft. **K. Vélon:** Methodology, Investigation, Data curation. **G. S. Bhatia:** Validation, Writing – review & editing. **A. Hejjaji:** Validation, Writing – review & editing. **A.J. Comer:** Conceptualization, Supervision, Funding acquisition, Writing – review & editing.

Declaration of Competing Interest

The authors declare that they have no known competing financial interests or personal relationships that could have appeared to influence the work reported in this paper.

Data availability

The raw/processed data required to reproduce these findings cannot be shared at this time as the data also forms part of an ongoing study

Acknowledgments

This work was supported by European Union's Horizon 2020 research and innovation programme under grant agreement No. 952966 (FIBREGY Project). The authors acknowledge the support received from Mr. Alex Portella and Mr. Adrian McEvoy, University of Limerick towards specimen fabrication and mechanical testing. The authors are also thankful to the School of Engineering, University of Limerick, Ireland for providing access to test equipment and software.

References

[1] Lande-Sudall D, Stallard T, Stansby P. Co-located offshore wind and tidal stream turbines: Assessment of energy yield and loading. Renew Energy 2018;118:627–43. https://doi.org/10.1016/j.renene.2017.10.063.
[2] Gourvenec S, Sturt F, Reid E, Trigos F. Global assessment of historical, current and forecast ocean energy infrastructure: Implications for marine space planning, sustainable design and end-of-engineered-life management. Renew Sustain Energy Rev 2022:154. https://doi.org/10.1016/j.rser.2021.111794.
[3] O'Leary K, Pakrashi V, Kelliher D. Optimization of composite material tower for offshore wind turbine structures. Renew Energy 2019;140:928–42. https://doi.org/10.1016/j.renene.2019.03.101.
[4] Summerscales J, Graham-Jones J, Pemberton R, editors. Marine Composites : Design and Performance (Woodhead Publishing Series in Composites Science and Engineering). Reprint ed. Duxford, UK: Woodhead Publishing, UK; 2018.
[5] Buck BH, Langan R, editors. Aquaculture perspective of multi-use sites in the open ocean: The untapped potential for marine resources in the anthropocene. 1st Edition. Cham, Switzerland: Springer; 2017. https://doi.org/10.1007/978-3-319-51159-7.
[6] Gupta R, Huo D, White M, Jha V, Stenning GBG, Pancholi K. Novel method of healing the fibre reinforced thermoplastic composite: A potential model for offshore applications. Compos Commun 2019;16:67–78. https://doi.org/10.1016/j.coco.2019.08.014.
[7] Gagani AI, Krauklis AE, Sæter E, Vedvik NP, Echtermeyer AT. A novel method for testing and determining ILSS for marine and offshore composites. Compos Struct 2019;220:431–40. https://doi.org/10.1016/j.compstruct.2019.04.040.
[8] Cadieu L, Kopp JB, Jumel J, Bega J, Froustey C. A fracture behaviour evaluation of Glass/Elium150 thermoplastic laminate with the DCB test: Influence of loading rate and temperature. Compos Struct 2021:255. https://doi.org/10.1016/j.compstruct.2020.112907.
[9] Chilali A, Zouari W, Assarar M, Kebir H, Ayad R. Analysis of the mechanical behaviour of flax and glass fabrics-reinforced thermoplastic and thermoset resins. J Reinf Plast Compos 2016;35:1217–32. https://doi.org/10.1177/0731684416645203.
[10] Obande W, Ó Brádaigh CM, Ray D. Continuous fibre-reinforced thermoplastic acrylic-matrix composites prepared by liquid resin infusion – A review. Compos Part B Eng 2021;215. https://doi.org/10.1016/j.compositesb.2021.108771.
[11] Gobikannan T, Portela A, Haldar AK, Nash NH, Bachour C, Manolakis I, et al. Flexural properties and failure mechanisms of infusible thermoplastic- and thermosetting based composite materials for marine applications. Compos Struct 2021;273:114276. https://doi.org/10.1016/j.compstruct.2021.114276.
[12] Nash NH, Portela A, Bachour-Sirerol CI, Manolakis I, Comer AJ. Effect of environmental conditioning on the properties of thermosetting- and thermoplastic-matrix composite materials by resin infusion for marine applications. Compos B Eng 2019:177. https://doi.org/10.1016/j.compositesb.2019.107271.
[13] Kazemi ME, Shanmugam L, Lu D, Wang X, Wang B, Yang J. Mechanical properties and failure modes of hybrid fiber reinforced polymer composites with a novel liquid thermoplastic resin, Elium®. Compos A Appl Sci Manuf 2019:125. https://doi.org/10.1016/j.compositesa.2019.105523.
[14] Obande W, Ray D, Ó Brádaigh CM. Viscoelastic and drop-weight impact properties of an acrylic-matrix composite and a conventional thermoset composite – A comparative study. Mater Lett 2019;238:38–41. https://doi.org/10.1016/j.matlet.2018.11.137.
[15] Barbosa LCM, Bortoluzzi DB, Ancelotti AC. Analysis of fracture toughness in mode II and fractographic study of composites based on Elium® 150 thermoplastic matrix. Compos B Eng 2019;175:107082.
[16] Ageyeva T, Sibikin I, Kovács JG. Review of thermoplastic resin transfer molding: Process modeling and simulation. Polymers (Basel) 2019:11. https://doi.org/10.3390/polym11101555.
[17] Bhudolia SK, Perrotey P, Joshi SC. Mode I fracture toughness and fractographic investigation of carbon fibre composites with liquid Methylmethacrylate thermoplastic matrix. Compos B Eng 2018;134:246–53. https://doi.org/10.1016/j.compositesb.2017.09.057.
[18] Lee HE, Chung YS, Kim SS. Feasibility study on carbon-felt-reinforced thermoplastic composite materials for PEMFC bipolar plates. Compos Struct 2017;180:378–85. https://doi.org/10.1016/j.compstruct.2017.08.037.
[19] Stavrov D, Bersee HEN. Resistance welding of thermoplastic composites-an overview. Compos A Appl Sci Manuf 2005;36:39–54. https://doi.org/10.1016/j.compositesa.2004.06.030.
[20] Jongbloed B, Teuwen J, Palardy G, Fernandez Villegas I, Benedictus R. Continuous ultrasonic welding of thermoplastic composites: Enhancing the weld uniformity by changing the energy director. J Compos Mater 2020;54:2023–35. https://doi.org/10.1177/0021998319890405.
[21] Kinvi-Dossou G, Matadi Boumbimba R, Bonfoh N, Garzon-Hernandez S, Garcia-Gonzalez D, Gerard P, et al. Innovative acrylic thermoplastic composites versus conventional composites: Improving the impact performances. Compos Struct 2019;217:1–13.
[22] Matadi Boumbimba R, Coulibaly M, Khabouchi A, Kinvi-Dossou G, Bonfoh N, Gerard P. Glass fibres reinforced acrylic thermoplastic resin-based tri-block copolymers composites: Low velocity impact response at various temperatures. Compos Struct 2017;160:939–51. https://doi.org/10.1016/j.compstruct.2016.10.127.
[23] Obande W, Mamalis D, Ray D, Yang L, Ó Brádaigh CM. Mechanical and thermomechanical characterisation of vacuum-infused thermoplastic- and thermoset-based composites. Mater Des 2019:175. https://doi.org/10.1016/j.matdes.2019.107828.
[24] Han N, Yuksel O, Zanjani JSM, An LL, Akkerman R, Baran I. Experimental Investigation of the Interlaminar Failure of Glass/Elium® Thermoplastic Composites Manufactured With Different Processing Temperatures. Appl Compos Mater 2022;29:1061–82. https://doi.org/10.1007/s10443-021-10000-5.
[25] Shah SZH, Megat-Yusoff PSM, Choudhry RS, Sajid Z, Din IU. Experimental investigation on the quasi-static crush performance of resin-infused thermoplastic 3D fibre-reinforced composites. Compos Commun 2021:28. https://doi.org/10.1016/j.coco.2021.100916.
[26] Murray RE, Penumadu D, Cousins D, Beach R, Snowberg D, Berry D, et al. Manufacturing and Flexural Characterization of Infusion-Reacted Thermoplastic Wind Turbine Blade Subcomponents. Appl Compos Mater 2019;26(3):945–61.
[27] Bhudolia SK, Gohel G, Kantipudi J, Leong KF, Gerard P. Mechanical performance and damage mechanisms of thin rectangular carbon/ Elium® tubular thermoplastic composites under flexure and low-velocity impact. Thin-Walled Struct 2021:165. https://doi.org/10.1016/j.tws.2021.107971.
[28] Bhudolia SK, Joshi SC, Bert A, Yi Di B, Makam R, Gohel G. Flexural characteristics of novel carbon methylmethacrylate composites. Compos Commun 2019;13:129–33. https://doi.org/10.1016/j.coco.2019.04.007.
[29] Raponi OdA, Barbosa LCM, de Souza BR, Ancelotti Junior AC. Study of the influence of initiator content in the polymerization reaction of a thermoplastic liquid resin for advanced composite manufacturing. Adv Polym Tech 2018;37(8):3579–87.
[30] ISO 527-5-2009 Plastics Determination of tensile properties -Test conditions for unidirectional fibre-reinforced plastic composites n.d.
[31] ISO 14125 - Fibre-reinforced plastic composites-Determination of flexural properties. 1998.
[32] ISO 14130 - Fibre-reinforced plastic composites - Determination of apparent interlaminar shear strength by short-beam method. 1997.
[33] ASTM D 3171-15 Standard Test Methods for Constituent Content of Composite Materials 1. n.d. https://doi.org/10.1520/D3171-15.
[34] Fan Z, Santare MH, Advani SG. Interlaminar shear strength of glass fiber reinforced epoxy composites enhanced with multi-walled carbon nanotubes. Compos A Appl Sci Manuf 2008;39:540–54. https://doi.org/10.1016/j.compositesa.2007.11.013.
[35] Liu Yu, Yang J-P, Xiao H-M, Qu C-B, Feng Q-P, Fu S-Y, et al. Role of matrix modification on interlaminar shear strength of glass fibre/epoxy composites. Compos B Eng 2012;43(1):95–8.
[36] Hernández S, Sket F, Molina-Aldareguía JM, González C, LLorca J. Effect of curing cycle on void distribution and interlaminar shear strength in polymer-matrix composites. Compos Sci Technol 2011;71(10):1331–41.